https://doi.org/10.5194/acp-2020-305
Preprint. Discussion started: 7 May 2020


Atmospheric Chemistry and Physics Discussions

# Decennial time trends and diurnal patterns of particle number concentrations in a Central European city between 2008 and 2018

Santtu Mikkonen[1,2], Zoltán Németh[3], Veronika Varga[3], Tamás Weidinger[4], Ville Leinonen[1], Taina Yli-Juuti[1], and Imre Salma[3]

[1] Department of Applied Physics, University of Eastern Finland, P.O. Box 1627, 70211 Kuopio, Finland
[2] Department of Environmental and Biological Sciences, University of Eastern Finland, P.O. Box 1627, 70211 Kuopio, Finland
[3] Institute of Chemistry, Eötvös University, H-1518 Budapest, P.O. Box 32, Hungary
[4] Department of Meteorology, Eötvös University, H-1518 Budapest, P.O. Box 32, Hungary

*Correspondence to*: Imre Salma (salma@chem.elte.hu) and Santtu Mikkonen (santtu.mikkonen@uef.fi)

**Abstract.** Multiple atmospheric properties were measured semi-continuously in the Budapest platform for Aerosol Research and Training Laboratory for a time interval of 2008-2018. Dataset of 6 full measurement years during a decennial time interval were subjected to statistical time trend analyses by an advanced dynamic linear model and a generalized linear mixed model. The main interest in the analysed data set was on particle number concentrations in the diameter ranges from 6 to 1000 nm ($N_{6–1000}$), from 6 to 100 nm ($N_{6–100}$, ultrafine particles), from 25 to 100 nm ($N_{25–100}$) and from 100 to 1000 nm ($N_{100–1000}$). These data were supported by concentrations of $SO_2$, CO, NO, $NO_x$, $O_3$, $PM_{10}$ mass, air temperature, relative humidity, wind speed, atmospheric pressure, global solar radiation, condensation sink, gas-phase $H_2SO_4$ proxy, classes of new aerosol particle formation (NPF) and growth events and meteorological macro-circulation patterns. The trend of the particle number concentrations derived as a change in the statistical properties of background state of the data set decreased in all size fractions over the years. Most particle number concentrations showed decreasing decennial statistical trends. The estimated annual mean decline of $N_{6–1000}$ was (4–5)% during the 10-year measurement interval, which corresponds to a mean absolute change of –590 $cm^{-3}$ in a year. This was interpreted as a consequence of the decreased anthropogenic emissions mainly from road traffic. Similar trends were not observed for the air pollutant gases. Diurnal statistical patterns of particle number concentrations showed tendentious variations, which were associated with typical diurnal activity–time pattern of inhabitants in cities, particularly of vehicular road traffic. The trend patterns for NPF event days contained a huge peak from late morning to late afternoon, which is unambiguously caused by NPF and growth processes. These peaks were rather similar to each other in the position, shape and area on workdays and holidays, which implies that the dynamic and timing properties of NPF events are not substantially influenced by anthropogenic activities in central Budapest. Diurnal pattern for $N_{25–100}$ exhibited the largest relative changes, which were related to particle emissions from high-temperature sources. The diurnal pattern for $N_{100–1000}$ – which represents chemically and physically aged particles of larger spatial scale – were different from the diurnal patterns for the other size fractions.

https://doi.org/10.5194/acp-2020-305
Preprint. Discussion started: 7 May 2020


Atmospheric Chemistry and Physics Discussions

## 1 Introduction

Atmospheric aerosol can be characterised by various properties. There are several important phenomena and processes in which individual particles play a role. In these cases, particle number concentrations or particle number size distributions are the relevant metrics. Number concentrations of (insoluble) particles produce adverse effects on human health (Oberdörster et al., 2005; Rich et al., 2012; Cassee et al., 2013; Braakhuis et al., 2014; Ostro et al., 2015; Schmid and Stoeger, 2016; Ohlwein et al., 2019). Individual particles and their properties are also important in cloud formation processes and, therefore, in indirect aerosol climate forcing (Makkonen et al., 2009; Merikanto et al, 2009; Sihto et al., 2011; Kerminen et al., 2012; Carslaw et al., 2013; Gordon et al., 2016). Particle numbers and associated size distributions are relevant properties in several optical interactions in the atmosphere (e.g. Moosmuller et al., 2009) and in various surface-controlled chemical reactions (e.g. Pöschl et al., 2007).

In the global troposphere, it is the new aerosol particle formation (NPF) and consecutive growth process that is the dominant source of particle numbers (Spracklen et al., 2006; Yu et al., 2010; Kulmala et al., 2013; Dunne et al., 2016). This source type occurs in various atmospheric environments around the world and produces secondary particles (Kerminen et al., 2018 and references therein). The major anthropogenic source of (primary) particles is combustion. It includes traffic exhaust mainly from diesel engines, fuel or waste burning in industrial and domestic installations, residential heating and cooking (Paasonen et al., 2016; Masiol et al., 2018). Nanotechnology and its products can have importance in some limited or occupational environments. In large cities and in longer time intervals, primary particles often prevail over secondary particles (Brines et al., 2015; Salma et al., 2017; Saha et al., 2018).

Ultrafine (UF) particles (with a diameter $d$<100 nm) account for most of the particle number concentrations but have usually negligible contribution to particulate matter (PM) mass. This implies that particle numbers are not covered by legislative regulations on the ambient air quality, which are ordinary based on the PM mass. Particle number concentrations have not been promulgated among the air quality standards yet. There are, however, mitigation policies and control regulations, which intend to reduce their ambient levels as part of an overall air-quality improvement strategy since 1990s. The legislations, for instance in the EU including Hungary, focus on the particle emissions from diesel engines (Giechaskiel et al., 2018). There were some important changes in the car emissions during the time interval under the investigation in this study. These included the introduction of Euro 5 and 6 regulations for light-duty vehicles in January 2011 and Euro VI regulations for heavy-duty vehicles in September 2015 (the number of emitted particles with diameters >23 nm should be $<6\times10^{11}$ km$^{-1}$ for type approval). A prerequisite for the efficient operation of exhaust after treatment devices is having fuel with low sulfur content. The reduction of sulfur in diesel fuel for on-road transport was decreased after several previous phases to <10 ppm in January 2009 (Directive 2009/30/EC). Sulfur content in fuels for mobile non-road diesel vehicles – including mobile machinery, agricultural and forestry

https://doi.org/10.5194/acp-2020-305
Preprint. Discussion started: 7 May 2020


Atmospheric Chemistry and Physics Discussions

tractors, inland waterway vessels and recreational crafts – was limited at a level of 1000 ppm from 2008 and at 10 ppm from 2011. The unsuitable/dangerous fuel types for domestic heating are also listed, their emission factors are determined, and the accumulated information is disseminated among potential users. As far as secondary particles are concerned, it is not straightforward to reduce their concentration levels because the effects of gaseous and aerosol species on the NPF are complex and uncertain due to nonlinear relationship and feedbacks in their related processes.

It is relevant to investigate the potential changes, namely overall and diurnal tendencies of particle number concentrations from different sources on longer run because of their role in both health-risk and climate-change issues. The major source types of particle numbers can be separated by measuring their size distributions. Atmospheric NPF events produce particles of the nucleation mode, which occurs intermittently, and which gradually merges into the larger Aitken mode. High temperature emission sources ordinarily produce Aitken-mode particles, while transformation processes (physical and chemical aging) of existing particles in the atmosphere give rise to the accumulation mode. An important property of the nucleation- and Aitken-mode particles is that their residence time is limited to several hours (Raes et al., 2000; Salma et al., 2011). This is different from accumulation-mode particles, which reside in the air up to 7 days. This means that the particles of the former two modes are present in the air until their sources are active, and that their concentrations can change substantially and rapidly over a day (e.g. Mikkonen et al., 2011a, Salma et al., 2014, 2017; Paasonen et al., 2016). This is advantageous when source types are to be identified or quantified. At the same time, the relatively short residence time is not beneficial when time trends are to be studied and derived. The limited residence time can cause additional, substantial and sudden variability in time with or without time patterns, which can complicate the evaluation.

Particle number concentrations or particle number size distributions in the relevant diameter range (i.e. from few nanometers to ca. 1 μm) are measured for various purposes. They include fundamental studies on atmospheric nucleation and particle growth phenomena, which usually require semi-continuous long-term measurements. The related experimental data sets have been accumulating gradually (Wehner and Wiedensohler, 2003; Asmi et al., 2013; Kerminen et al., 2018; Nieminen et al., 2018). They can also be exploited for time trend analysis by using appropriate statistical models. At present, however, knowledge on time trends particularly in various size fractions and over several years is largely lacking with few recent exceptions (Masiol et al., 2018; Saha et al., 2018; Sun et al., 2019).

Research activities dedicated to NPF and growth events in Budapest have been going on since November 2008. Measurements for 6 full years were realised in the city centre at a single fixed location. Semi-continuous and critically evaluated data sets consisting of particle number size distributions, concentrations of criteria air pollutants and meteorological data were available for the study. They were combined in a coherent set, which was utilised in two statistical models developed specifically to

https://doi.org/10.5194/acp-2020-305
Preprint. Discussion started: 7 May 2020


Atmospheric Chemistry and Physics Discussions

determine the time trends for particle number concentrations in several important size fractions from 2008 to 2018. The main objectives of this study are to present and discuss the statistical models, to interpret their results on time trends and diurnal variability, to quantify the change rates, and to relate the temporal tendencies to different atmospheric sources, processes and environmental circumstances.

## 2 Methods

### 2.1 Measurements

Most experimental data dealt with in the present study were obtained at a single urban site, namely at the Budapest platform for Aerosol Research and Training (BpART) research laboratory (N 47° 28' 29.9", E 19° 3' 44.6", 115 m above mean sea level). This location represents a well-mixed, average atmospheric environment for the city centre of Budapest due to its geographical and meteorological conditions (Salma et al., 2016a). The local emissions include diffuse urban traffic exhaust, household/residential emissions and limited industrial sources together with some off-road transport (diesel rail, shipping and airplane emissions). Experimental data for 6 full-year-long time intervals, i.e. from 3 November 2008 to 2 November 2009, from 13 November 2013 to 12 November 2014, from 13 November 2014 to 12 November 2015, from 13 November 2015 to 12 November 2016, from 28 January 2017 to 27 January 2018 and from 28 January 2018 to 27 January 2019 were available for this single site. A decennial time interval from 03 November 2008 to 02 November 2018 was considered in the statistical analysis. Local time (LT=UTC+1 or daylight-saving time, UTC+2) was chosen as the time base of the data processing because the ordinary daily activities of inhabitants substantially influence the atmospheric concentrations and several processes in cities (Salma et al., 2014).

The major aerosol measuring system was a flow-switching type differential mobility particle sizer (DMPS, Alto et al., 2001). It records particle number concentrations in an electrical mobility diameter range from 6 to 1000 nm in the dry state of particles (with a relative humidity of RH<30%) in 30 channels (Salma et al., 2011). The measuring system was updated twice; in spring 2013 and winter 2016. Its major parts including a differential mobility analyser (DMA, Hauke-type with a length of 28 cm) and a condensation particle counter (CPC, TSI model 3775) remained, however, unchanged. They were cleaned and serviced. The diameter resolution of the DMA was also calibrated during the updates. Several data validation or comparative exercises were realised over the years; the most extensive inter-comparison was realised in summer 2015 (Salma et al., 2016a) and autumn 2019. The time resolution of the DMPS measurements was approximately 10 min in the year 2008–2009 and it was 8 min from 13 November 2013 on. The sampling inlet was installed at a height of 12.5 m above the street level. There was no upper-size cut-off inlet applied to the sampling line, and a rain shield and insect net were only adopted. The measurements were performed according to the international technical standard (Wiedensohler et al., 2012).

https://doi.org/10.5194/acp-2020-305
Preprint. Discussion started: 7 May 2020


Atmospheric Chemistry and Physics Discussions

Meteorological data for air temperature ($T$), relative humidity (RH), wind speed (WS), wind direction and atmospheric pressure ($p$) were obtained from a measurement station of the Hungarian Meteorological Service (HMS) operated in a distance of ca. 70 m from the BpART laboratory by standardised methods (Vaisala HMP45D humidity and temperature probe, Vaisala WAV15A anemometer, Vaisala pressure, all Finland) with a time resolution of 10 min. Global solar radiation (GRad) data were measured by a CMP11 pyranometer (Kipp and Zonnen, The Netherlands) at another station of the HMS situated in 10 km in Eastern direction with a time resolution of 1 h. Concentrations of pollutants $SO_2$, CO, NO, $NO_x$, $O_3$, and $PM_{10}$ mass were acquired from a measurement station of the National Air Quality Network in Budapest in Széna Square, which is located in the upwind prevailing wind direction in a distance of 4.5 km from the BpART laboratory. They are measured by UV fluorescence (Ysselbach 43C), IR absorption (Ysselbach 48C), chemiluminescence (Thermo 42C), UV absorption (Ysselbach 49C) and beta-ray attenuation (Thermo 5014I) methods, respectively with a time resolution of 1 h.

The availability of the DMPS data over the six one-year-long time intervals were 95, 99, 95, 73, 99 and 90%, respectively. The meteorological data were accessible in >90% of time in each year, while the concentration data for key pollutants were available in >85% of the yearly time intervals.

### 2.2 Data treatment

Particle number concentrations in the diameter ranges 1) from 6 to 1000 nm ($N_{6–1000}$), 2) from 6 to 100 nm ($N_{6–100}$), 3) from 25 to 100 nm ($N_{25–100}$) and 4) from 100 to 1000 nm ($N_{100–1000}$) were calculated from the measured and inverted DMPS data. The size ranges were selected to represent 1) the total particles, 2) UF particles, 3) UF particles emitted mainly from incomplete combustion (and partially grown by condensation; this size ranges is dominated by primary particles in cities in most of the time) and 4) physically and chemically aged particles which usually represent larger spatial extent, respectively (Salma et al., 2014, 2017).

Condensation sink (CS) for vapour molecules onto the surface of existing aerosol particles was calculated for discrete size distributions (Kulmala et al., 2001, 2012; Dal Maso et al., 2002, 2005). Dry particle diameters were considered in the calculations and condensing vapour was assumed to have sulphuric acid properties.

One of the key components for NPF events is the gas-phase $H_2SO_4$ (Sipilä et al., 2010; Sihto et al., 2011). It is challenging to measure its atmospheric concentration and, therefore, the experimental data for long time intervals are rare. The relative effects of gas-phase $H_2SO_4$ are, however, often estimated by deriving its proxy value. In this study, the $H_2SO_4$ proxy was calculated according to Mikkonen et al. (2011b), where the best proxy was based on GRad, $SO_2$ concentration, RH and CS. The proxy is defined for GRad>10 W $m^{-2}$. Other widely used proxy was introduced by Petäjä et al. (2009), but that was

https://doi.org/10.5194/acp-2020-305
Preprint. Discussion started: 7 May 2020


Atmospheric Chemistry and Physics Discussions

created for clean boreal forest environment. The most recent proxy from Dada et al. (2020) is currently under review and has not been tested against the proxy used here. All experimental data were used with their maximum time resolution.

The influence of large-scale weather types was considered on a daily basis by including codes for macro-circulation patterns (MCPs) invented specifically for the Carpathian Basin (Péczely, 1957; Károssy, 2016). The classification is based on the extension and development of cyclones and anticyclones relative to the Carpathian Basin via the daily sea-level pressure maps constructed for 00:00 UTC in the North-Atlantic–European region. Basic information on the MCPs are summarised in Table 1.

**Table 1.** Macro-circulation patterns (Péczely codes) and their seasonal and annual occurrences in the Carpathian Basin for years 1958–2010 (Maheras et al., 2018).

| No. | Code | Description | Occurrence (%) | | | | |
|---|---|---|---|---|---|---|---|
| | | | Winter | Spring | Summer | Autumn | Annual |
| 1 | mCc | Cyclone with a cold front over NE Europe, N wind | 7.3 | 11.3 | 12.1 | 8.0 | 9.7 |
| 2 | AB | Anticyclone over the British Isles, N wind | 5.6 | 7.1 | 8.6 | 6.4 | 6.9 |
| 3 | CMc | Mediterranean cyclone with a cold front over S Europe, N wind | 2.5 | 3.5 | 1.8 | 1.9 | 2.4 |
| 4 | mCw | Mediterranean cyclone with a warm front over NE Europe, S wind | 9.2 | 9.7 | 5.7 | 7.2 | 7.9 |
| 5 | Ae | Anticyclone over E Europe, S wind | 14.2 | 11.3 | 7.3 | 17.6 | 12.6 |
| 6 | CMw | Mediterranean cyclone with a warm front over S Europe, S wind | 8.9 | 8.7 | 3.7 | 8.3 | 7.4 |
| 7 | zC | Highly developed cyclone over N Europe, W wind | 5.0 | 3.2 | 2.7 | 2.9 | 3.5 |
| 8 | Aw | Anticyclone over W Europe, W wind | 13.1 | 11.2 | 20.8 | 12.8 | 14.6 |
| 9 | As | Anticyclone over S Europe, W wind | 7.0 | 4.4 | 2.9 | 5.6 | 4.9 |
| 10 | An | Anticyclone over N Europe, E wind | 10.9 | 12.8 | 11.3 | 10.1 | 11.3 |
| 11 | AF | Anticyclone over Fennoscandia, E wind | 2.8 | 5.2 | 5.9 | 3.7 | 4.4 |
| 12 | A | Anticyclone over the Carpathian Basin, changing wind direction | 11.8 | 7.3 | 13.3 | 13.3 | 11.4 |
| 13 | C | Cyclone over the Carpathian Basin, changing wind direction | 1.7 | 4.3 | 3.9 | 2.2 | 3.0 |

Each data line containing the date and time, concentrations, CS, $H_2SO_4$ proxy, meteorological data and MCP codes was further labelled by several indices on a daily basis. These labels served to differentiate between various environmental conditions, which can lead to substantial changes in some variables (Salma et al., 2014). The workdays were marked by label WD, while the holidays were denoted by label HD. Varying classes of NPF event days were also labelled differently. The classification was

https://doi.org/10.5194/acp-2020-305
Preprint. Discussion started: 7 May 2020


Atmospheric Chemistry and Physics Discussions

accomplished via the particle number size distribution surface plots (Dal Maso et al., 2005; refined in Németh et al., 2018 for urban sites) on a daily basis. The main classes were: NPF event days (marked by label NPF), non-event days (label NE), days with undefined character and days with missing data. The earliest estimated time of the beginning of a nucleation ($t_1$) was also derived (Németh and Salma, 2014) and was added to the data record as a parameter. Finally, the data lines were labelled according to the actual technical status of the DMPS system. The data obtained from the beginning of the measurements to the 1st update was labelled as S1, the data derived between the 1st and 2nd updates were label as S2, and label S3 was given to the data obtained after the 2nd update.

### 2.3 Statistical modelling

Atmospheric data are usually not normally distributed, and, therefore, non-parametric methods are often used to detect their long-term trends (Asmi et al., 2013; Masiol et al., 2018). The coherent data set prepared as described in Sect. 2.2 was analysed in two ways. First, time trends for concentrations of particles and air pollutants were estimated by using a dynamic linear model (DLM) method. Secondly, the factors affecting the changes in particle concentrations were detected with a generalized linear mixed model (GLMM).

#### 2.3.1 Dynamic linear model

Dynamic linear models (Durbin and Koopman, 2012; Petris et al., 2009; Laine, 2020) are state-of-the-art tools for time trend detection. The trend is seen as a statistical change in the properties of the background state of the system. Although changes in aerosol concentrations have previously been approximated with linear trends (e.g. Sun et al., 2019), this is not always the most suitable method since the processes affecting the concentrations are continuously evolving over time. Additionally, time series of atmospheric measurements can include multiple time-dependent cycles (e.g. seasonal and diurnal cycles) which are typically non-stationary – meaning that their distributional properties change over time. The DLM approach effectively decomposes the data series into basic components such as level, trend, seasonality and effect of external forcing by describing statistically the underlying structure of the process that generated the measured data. All these components are defined by Gaussian distributions, and they are allowed to vary in time, and the significance and magnitude of this variation can also be modelled and estimated. In the basic setup of DLM, the sign or the magnitude of the trend is not defined in advance by the model formulation but estimated from the data. The method can detect and quantify trends, but the explanations for the observed changes is provided by the user. Nevertheless, it determines if the observations are consistent with the selected model. We used the DLM to explain variability in the particle concentration time series using following components: locally linear mean level, trend, seasonal effect, autoregressive component and noise. The evolution of the investigated concentrations – after the seasonal and noise components were filtered out – is modelled by using the smoothed mean

https://doi.org/10.5194/acp-2020-305
Preprint. Discussion started: 7 May 2020


Atmospheric Chemistry and Physics Discussions

level. Here, the change in the mean level is the trend of the variable. The statistical model can be described by the following equations (Mikkonen et al., 2015):

$$y_t = \mu_t + \gamma_t + \eta_t + \varepsilon_{obs}\ ,\ \varepsilon_{obs} \sim N(0, \sigma_t^2), \quad (1)$$

$$\mu_t = \mu_{t-1} + \alpha_t + \varepsilon_{level},\ \varepsilon_{level} \sim N(0, \sigma_{level}^2), \quad (2)$$

$$\alpha_t = \alpha_{t-1} + \varepsilon_{trend},\ \varepsilon_{trend} \sim N(0, \sigma_{trend}^2), \quad (3)$$

where $y_t$ is the investigated concentration at time $t$, $\mu_t$ is the mean level and $\alpha_t$ is the change in the level from time $t$–1 to time $t$, $\gamma_t$ is the seasonal component and $\eta_t$ is an autoregressive error component. Here, this latter level is fixed. The Gaussian stochastic $\varepsilon$ terms are used for the observation uncertainty and for random dynamics of the level and the trend. The seasonal component $\gamma_t$ contains dummy variables for each month, so it has a different value for each month with a condition that 12 consecutive months sum to zero. More detailed description on how the model is written through state space equation can be found in Mikkonen et al. (2015).

### 2.3.2 Generalized linear mixed model

Linear mixed models (McCulloch et al., 2008) belong to the family of models that combine several different kinds of models used in multivariate analysis when the data do not fulfil the standard independency and homogeneity assumptions. This is the normal case with atmospheric and climatological measured variables (e.g. Mikkonen et al., 2011a). The main goal of the mixed models is to estimate not only the mean of the measured response variable but also the variance-covariance structure of the data, which makes the model more valid for complex atmospheric data. In addition, modelling the (co)variances of the variables reduces the bias of the estimates, and prevents autocorrelation of the residuals. The model is constructed from general linear model, written in matrix format as $\boldsymbol{y}=\mathbf{X}\boldsymbol{\beta}+\boldsymbol{\varepsilon}$, by adding a so-called random component (denoted $\boldsymbol{Zu}$) to the model, thus the model is given by $\boldsymbol{y}= \mathbf{X}\boldsymbol{\beta}+\boldsymbol{Zu}+\boldsymbol{\varepsilon}$. Here, if we let $n$ equal to number of observations, $p$ equal to number of fixed parameters and $q$ equal to number of random parameters in the model, $\boldsymbol{y}$ is the ($n$×1) vector of measurements of the variable of interest, $\boldsymbol{\beta}$ denotes the unknown ($p$×1) vector of intercept and slope estimates of the model, $\mathbf{X}$ is the ($n$×$p$) matrix of observations from predictor variables and $\boldsymbol{\varepsilon}$ contains the residuals of the model. In the random part, $\mathbf{Z}$ is the ($n$×$q$) design matrix for the ($q$×1) vector of random covariates $\boldsymbol{u}$ with a $q$-dimensional normal distribution. With adequate choices of the matrix $\mathbf{Z}$, different covariance structures Cov($u$)=$\mathbf{G}$ and Cov($\boldsymbol{\varepsilon}$)=$\mathbf{R}$ can be defined and fitted. Successful modelling of variances and covariances of the observations provides valid statistical inference for the fixed effects $\boldsymbol{\beta}$ of the mixed model. In contrast to general linear models, the error terms $\boldsymbol{\varepsilon}$ can be correlated, which makes the modelling more robust. It follows from this that the distribution of observations can be described by a normal distribution with the expectation of $\bar{\mathbf{X}}$ and covariance matrix $\mathbf{V}$, which is given by $\mathbf{V}=\mathbf{ZGZ}'+\mathbf{R}$. With GLMM, it is possible to reliably detect the factors which affect particle number

https://doi.org/10.5194/acp-2020-305
Preprint. Discussion started: 7 May 2020


Atmospheric Chemistry and Physics Discussions

concentrations or which act as indicators for their different sources. The model can be expressed in a mathematical form as (Mikkonen et al., 2011a):

$$N_{Di} = (\beta_0 + \beta_{setup} + u_m) + \alpha_d + (\beta_{wd} \cdot \beta_E) \cdot X_{Ti} + (\beta_1 + v_{1m}) \cdot \mathrm{SO_{2,i}} + (\beta_2 + v_{2m}) \cdot \mathrm{NO_{2,i}} + (\beta_3 + v_{3m}) \cdot \mathrm{O_{3,i}} + \beta_4 \cdot \mathrm{GRad_i} + \beta_5 \cdot \mathrm{RH_i} + \beta_6 \cdot \mathrm{MCP_i}, \quad (4)$$

where $N_{Di}$ is the number concentration in selected size range in time $i$, $\beta_0$ is a model intercept, $\beta_{setup}$ is a correction term for changes in the measurement system due to two major upgrades, $u_m$ is vector of random intercepts different for each month, $\alpha_d$ is average change of $N_{Di}$ per day (i.e. slope of trend), $\beta_{wd}$ and $\beta_E$ are coefficients for workday and NPF event day, respectively, and $X_{Ti}$ is the corresponding vector showing the type of the day (in both means: WD/HD and E/NE) in time $i$, $\beta_1 - \beta_5$ are fixed coefficients for $SO_2$, $NO_2$, $O_3$, *GRad* and *RH*, respectively, $\beta_6$ is the vector of coefficients for different macro-circular patterns (MCP) and $v_m$ are the random, month specific slopes for $SO_2$, $NO_2$, $O_3$ and *GRad*. The coefficients of the model can be interpreted in a similar manner as multivariate regression or general linear models, just with an addition of month-specific effects for given variables.

## 3 Results and discussion

An overview on annual averages of the data analysed in this study is given in Table 2. Annual insolation, which expresses the total energy density at the receptor site, was derived from the individual $\mathrm{GRad_i}$ data as $Q = n_\mathrm{d} \times 24 \times 3600 \times \sum_\mathrm{i} \mathrm{GRad_i}$ over the year of interest ($n_\mathrm{d}$ is the number of day in the year). Since the major sources of particles in cities include road vehicles and atmospheric nucleation, we added some indicative data on these specific sources as well. The median particle number concentrations are basically in line with many other comparable cities in the world (e.g. Kerminen et al., 2018; Masiol et al., 2018). They indicate a decreasing change (except for $N_{100–1000}$) over the years 2008–2018. At the same time, the annual averages of the other concentrations, meteorological data and auxiliary variables did not change substantially. Annual mean relative occurrence frequency of NPF events stayed almost constant with a mean and SD of (20±4)%, except for the measurement year 2015–2016 when it was unusually small. It is worth adding that the NPF increases the existing particle number concentrations in Budapest by a factor of approximately 2 on event days (Salma et al., 2017). The annual medians for the particle formation rate and particle growth rate also stayed constant and seemingly varied only as fluctuations within ca. ±20% and ±8%, respectively. The number of passenger cars was registered in Budapest remained constant within ±5%, while the share of the diesel-powered passenger cars increased modestly by a rate of approximately 12% from 2008 to 2018 (KSH, 2019). The number (ca. 4000) of buses registered in Budapest and the share (98%) of the diesel-power buses on the national bus fleet remained constant.

https://doi.org/10.5194/acp-2020-305
Preprint. Discussion started: 7 May 2020


Atmospheric Chemistry and Physics Discussions

**Table 2.** Annual medians of particle number concentrations in the diameter ranges from 6 to 1000 nm ($N_{6–1000}$), from 6 to 100 nm ($N_{6–100}$), from 25 to 100 nm ($N_{25–100}$) and from 100 to 1000 nm ($N_{100–1000}$), concentrations of $SO_2$, CO, NO, $NO_x$, $O_3$, $PM_{10}$ mass, annual means of air temperature ($T$), relative humidity (RH), wind speed (WS), atmospheric pressure ($P$) and annual insolation ($Q$), annual mean relative occurrence frequency of nucleation ($f_{NPF}$), annual median formation rate of particles with a diameter of 6 nm ($J_6$), annual median growth rate of particles with a diameter of 10 nm ($GR_{10}$; for the rates, see Salma and Németh, 2019), number of passenger cars registered in Budapest (Cars), the mean age and the share of diesel-powered vehicles (Diesel) separately for the 1-year-long measurement time intervals.

| Variable | Unit | 2008–2009 | 2013–2014 | 2014–2015 | 2015–2016 | 2017–2018 | 2018–2019 |
|---|---|---|---|---|---|---|---|
| $N_{6–1000}$ | $10^3$ cm$^{-3}$ | 11.5 | 9.7 | 9.3 | 7.5 | 8.6 | 8.3 |
| $N_{6–100}$ | $10^3$ cm$^{-3}$ | 9.1 | 7.2 | 6.9 | 5.7 | 6.8 | 6.5 |
| $N_{25–100}$ | $10^3$ cm$^{-3}$ | 5.1 | 4.3 | 4.1 | 3.3 | 3.6 | 3.2 |
| $N_{100–1000}$ | $10^3$ cm$^{-3}$ | 1.79 | 2.2 | 2.0 | 1.56 | 1.49 | 1.53 |
| $SO_2$ | μg m$^{-3}$ | 5.0 | 4.8 | 4.6 | 4.8 | 4.5 | 5.2 |
| CO | μg m$^{-3}$ | 547 | 488 | 577 | 513 | 534 | 624 |
| NO | μg m$^{-3}$ | 13.3 | 19.2 | 23 | 17.6 | 20 | 17.0 |
| $NO_x$ | μg m$^{-3}$ | 58 | 80 | 89 | 72 | 79 | 73 |
| $O_3$ | μg m$^{-3}$ | 23 | 14.8 | 19.6 | 25 | 20 | 21 |
| $PM_{10}$ | μg m$^{-3}$ | 33 | 31 | 39 | 29 | 28 | 36 |
| $T$ | °C | 12.0 | 13.2 | 13.2 | 12.9 | 13.2 | 13.3 |
| RH | % | 64 | 69 | 64 | 69 | 63 | 67 |
| WS | m s$^{-1}$ | 2.5 | 2.6 | 2.8 | 2.7 | 2.9 | 2.5 |
| $P$ | hPa | 1001 | 1003 | 1005 | 1004 | 1004 | 1004 |
| $Q$ | GJ m$^{-2}$ y$^{-1}$ | 4.75 | 4.51 | 4.71 | 4.67 | 4.95 | 4.81 |
| $f_{NPF}$ | % | 24 | 20 | 23 | 13.0 | 23 | 20 |
| $J_6$ | cm$^{-3}$ s$^{-1}$ | 4.2 | 3.5 | 4.4 | 4.6 | 6.3 | 5.3 |
| $GR_{10}$ | nm h$^{-1}$ | 7.6 | 6.6 | 6.5 | 8.0 | 7.5 | 7.5 |
| Cars* | $10^3$ pcs | 582 | 573 | 584 | 597 | 634 | 659 |
| Age* | y | 10.8 | 13.0 | 13.4 | 13.7 | 14.1 | 14.2 |
| Diesel* | % | 20 | 24 | 26 | 28 | 29 | n.a. |

* Status at the end of years 2009, 2013, 2014, 2015, 2017 and 2018, respectively.
n.a.: not yet available.

### 3.1 Decennial time scale

Overall statistical time trends for particle number concentrations in various size fractions obtained by the DLM are displayed in Figure 1. The curves confirm that the $N_{6–1000}$, $N_{6–100}$ and $N_{25–100}$ indeed decreased in Budapest between 2008 and 2018, while the change in $N_{100–1000}$ was not significant. The decline mostly took place in a monotonical manner except for perhaps the interval of summer 2016–spring 2017, when some partial/local increase could be realised for $N_{6–1000}$ and $N_{6–100}$.

https://doi.org/10.5194/acp-2020-305
Preprint. Discussion started: 7 May 2020


Atmospheric Chemistry and Physics Discussions

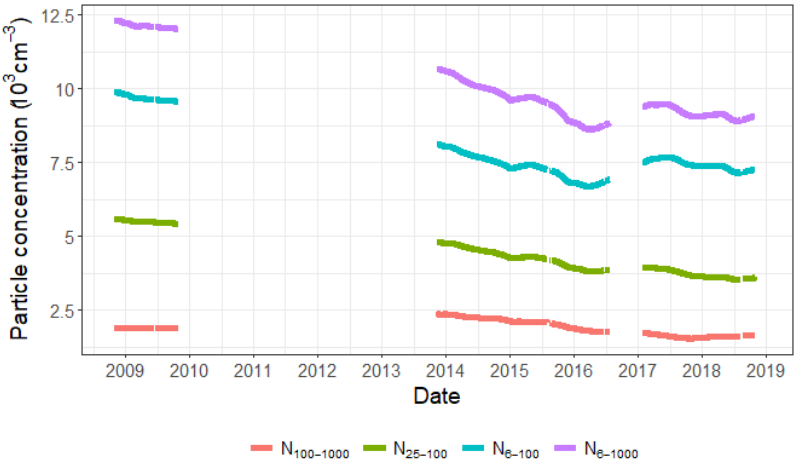


306 **Figure 1.** Statistical time trends of particle number concentrations in the diameter ranges from 6 to 1000 nm ($N_{6-1000}$), from 6 to 100 nm ($N_{6-100}$), from 25 to 100 nm ($N_{25-100}$) and from 100 to 1000 nm ($N_{100-1000}$) derived by DLM over a decennial interval.

309 There are several important sources, sinks and atmospheric transformation processes including
310 environmental conditions which can influence the atmospheric concentrations. The major sources
311 include both high-temperature emissions and NPF events as discussed in Sect. 1. The latter source is
312 affected by concentrations of precursor and other trace gases, meteorological properties for
313 photochemical reactions, and the interactions among gas-phase chemical species of different origin/type
314 with respect the formation yield of condensing vapours (Kulmala et al., 2014; McFiggans et al., 2019).
315 The air pollutants listed in Table 2 and gas-phase $H_2SO_4$ proxy – which are known or expected to affect
316 particle number concentrations – did not exhibit decreasing statistical trend between 2008 and 2018
317 (Fig. 2). On one hand, this decoupling confirms that the causes of the decrease in particle number
318 concentrations are not primarily related to meteorological conditions because they would jointly affect
319 the gas concentrations as well (if their sources are more-or-less constant over a certain time interval).
320 On the other hand, the constant gas concentrations suggest that the decreasing trend in particles does not
321 seem to be related to the major precursors or interacting gaseous chemical species (such as $SO_2$, $H_2SO_4$
322 or $NO_2$).
323

https://doi.org/10.5194/acp-2020-305
Preprint. Discussion started: 7 May 2020


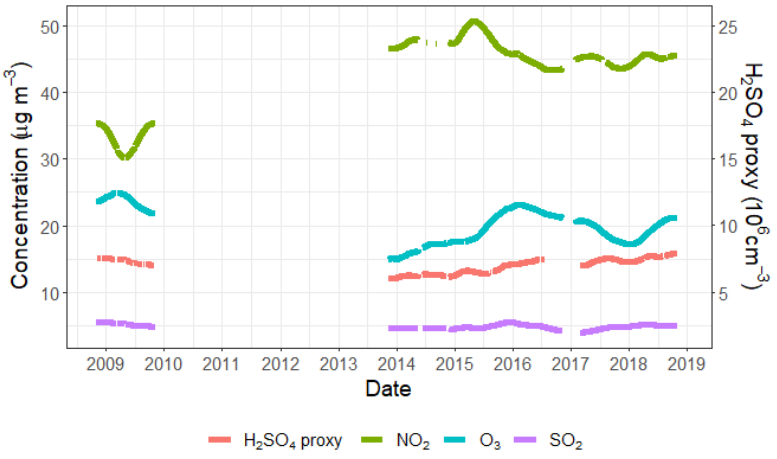


**Figure 2.** Statistical time trends of gas-phase $H_2SO_4$ proxy, $SO_2$, $O_3$ and $NO_2$ derived by DLM over the decennial interval.

As far as the meteorological conditions are concerned, some of them such as WS, boundary mixing layer height and *T* have previously been shown to influence the temporal variation of aerosol particles (e.g. Birmili et al., 2001; Mikkonen et al., 2011a). The annual means of possibly relevant properties and parameters in Table 2 – except for the particle number concentrations (which are under the investigation) and the fraction of diesel cars – did not show any obvious dependency; they virtually stayed constant over the years of interest. The possible effect of different weather conditions on the concentrations are studied separately by the GLMM and are discussed in Sect. 3.2.2. There were also no substantial and extensive urban constructions in the area (which could influence the urban air flow) nor larger systematic changes in the traffic circulation around the sampling site in the time interval considered. Therefore, the decline in the particle number concentrations is most likely interpreted as a consequence of the decreased anthropogenic particulate emissions in Budapest. The related source sectors can include vehicular road traffic and household heating/cooking. The decline happened at an increasing share of the diesel passenger cars and straitened emission control on (diesel) vehicles.

The average decrease rates of particle number concentrations as derived from both the DLM and GLMM statistical approaches are summarised in Table 3. The rates are shown as obtained from the models and scaled for the 10-year measurement interval to ensure the comparability of the slopes. The relative mean changes in % per year were expressed with respect to the starting value (mean of the first year). There are some differences between the corresponding results of the two models, which were caused by standardising the concentrations with the predictors in the models and by handling the upgrades of measurement setup differently. The changes in all size fractions were on the same level and only minor differences could be seen. As the estimates always contain some uncertainty, these differences are not considered as statistically significant. The largest difference between the two models was observed for

https://doi.org/10.5194/acp-2020-305
Preprint. Discussion started: 7 May 2020


Atmospheric Chemistry and Physics Discussions

$N_{100–1000}$ (which had the lowest absolute concentrations). One possible cause for this might be that GLMM standardises the results for variables indicating anthropogenic emissions and thus the size fraction that is the most sensitive for the emissions has the strongest effect. Considering all these, the rates from the two statistical models agree well. Furthermore, the rates for $N_{6–1000}$ and $N_{6–100}$ were identical. This is explained by the fact that these two size fractions are strongly connected; the typical $N_{6–100}/N_{6–1000}$ mean ratio in central Budapest is 75–80% (Salma and Németh, 2019). Small difference was also seen for $N_{25–100}$. In urban areas, this size fraction is mainly composed of particles from high-temperature emission sources. The source types responsible for the observed decline are further discussed in Sect. 3.2.1.

**Table 3.** Decrease rates of particle number concentrations in the diameter ranges from 6 to 1000 nm, from 6 to 100 nm, from 25 to 100 nm and from 100 to 1000 nm obtained by the dynamic linear model and generalized linear mixed model as a mean absolute change per year during the 10-year measurement interval and as a relative mean change per year with respect to the mean value of the first year.

| Size fraction (nm) | Dynamic linear model | | Generalized linear mixed model | |
|---|---|---|---|---|
| | Mean change/year ($cm^{-3}$) | Relative mean change (%/year) | Mean change/year ($cm^{-3}$) | Relative mean change (%/year) |
| 6–1000 | –510 | –4 | –660 | –5 |
| 6–100 | –400 | –4 | –480 | –5 |
| 25–100 | –310 | –6 | –360 | –5 |
| 100–1000 | –50 | –3 | –180 | –8 |

Our results concerning the decennial change rates (and our conclusions with regard to their causes mainly discussed in Sect. 3.2.1) are comparable and are in line with some other very recent studies. Sun et al. (2019) investigated the statistical concentration trends in particle numbers (and equivalent black carbon mass) at multiple urban, rural or background sites within the German Ultrafine Aerosol Network. Decreasing annual slopes of –(7.0–1.7)% were obtained for several size fractions (which are different from our intervals), and the most likely factors for the decreasing trends were assigned to declining anthropogenic emissions due to emission mitigation policies of the EU. Masiol et al. (2018) evaluated statistical time trends of particle number concentrations in various size fractions (which are different again from the previous and present studies) in Rochester, NY, USA, and obtained a typical decline rate of –4.6% per year for total particles. These outcomes and our data as well seem to be different from the results obtained by Saha et al. (2018) in the urban Pittsburgh, PA, USA by comparing two intervals of 2001–2002 and 2016–2017. It should be mentioned that in the latter research, the experimental setup for measuring particle number size distributions had a lower diameter limit of detection at 11 nm, some methodological approaches (e.g. classification of events) were different from ours and that the time trend was not derived by statistical modelling. The authors concluded that both the frequency of NPF events and their dynamic properties were reduced by (40−50)% over the past 15 years, resulting in ca. 48%

https://doi.org/10.5194/acp-2020-305
Preprint. Discussion started: 7 May 2020


Atmospheric Chemistry and Physics Discussions

reduction of UF concentrations. The changes were attributed to dramatic reductions in $SO_2$ emissions in the larger region.

### 3.2 Diurnal time scale

Diurnal statistical patterns of the particle number concentrations in different size fractions were predicted by the GLMM considering the following variables: GRad, RH, concentrations of $SO_2$, $NO_2$, $O_3$, and labels for workdays/holidays, for NPF event days/non-event days and for MCP codes. The initial screening for possible prediction variables was done in earlier papers. Studies such as Hyvönen et al. (2005), Mikkonen et al. (2006) and Nieminen et al. (2014) suggested that meteorological and trace gas variables affect NPF. Furthermore, e.g. Mikkonen et al. (2011a), Guo et al. (2012) and Zaidan et al. (2018) studied the factors which influence the growth of freshly formed particles as well as the concentrations of particles in larger size fractions and specified the possible predictors. All variables found in these screenings and measured at our site were tested one-by-one in the GLMM model in a stepwise manner. In each step, the significance of the added or removed variable was investigated by a likelihood ratio test (e.g. Pinheiro and Bates, 2000) until the final model shown in Eq. 4 was formed. The effect of the $H_2SO_4$ proxy was also tested, and the results for the daytime concentrations were similar to those obtained with the selection of variables above. The modelling results for night-time were, however, biased since the proxy is defined for GRad>10 W $m^{-2}$, and, therefore, we decided not to include the proxy into the final model.

#### 3.2.1 Diurnal statistical patterns

Modelled diurnal pattern of particle number concentrations for event days on workdays, event days on holidays, non-event days on workdays and non-event days on holidays separately for different size fractions are shown in Fig. 3. The curves on Fig. 3a–c resemble tendentious variations, which can be associated with typical diurnal activity–time pattern of inhabitants in cities, particularly with road traffic. They are also perfectly in line with the mean diurnal tendencies of experimentally determined concentrations in central Budapest (Salma et al., 2014; 2017) and are consistent with the time variations in many other European cities (Hussein et al., 2004; Aalto et al., 2005; Moore et al., 2007; Avino et al., 2011; Dall'Osto et al., 2013).

In the statistical diurnal patterns of UF particles (Fig. 3b), there is a huge peak from late morning to late afternoon on event days. This is unambiguously caused by NPF and growth process. The peaks on workdays and holidays are rather similar to each other in the position, shape and magnitude (area), which means that the dynamics and timing of NPF events in general are not substantially influenced by anthropogenic activities, which are more intensive on workdays than on holidays. It is worth mentioning that the overall contribution of the NPF to particle number concentrations is less than what is seemingly indicated by the diurnal patterns alone since NPF events occur on approximately 20% of days (Table 2).

https://doi.org/10.5194/acp-2020-305
Preprint. Discussion started: 7 May 2020


Atmospheric Chemistry and Physics Discussions

Emissions from vehicular road traffic is represented by a notable peak during the morning rush hours (between 05:30 and 08:30) on workdays. It is noted that the boundary layer mixing height is usually increased during this interval because of the increasing solar radiation intensity and mixing intensity. Another peak occurred around 21:00, thus later than the afternoon rush, which usually happens between 16:30 and 18:30. Under strong anti-cyclonic conditions, the evolution of the boundary layer mixing height and mixing intensity can decrease the concentration levels in the afternoons until sunset, and this can compensate the increased intensity of emissions. This all means that the afternoon peak is realised in a fuzzy manner since it is more influenced by local meteorology than by vehicular emissions. The effect of residential heating and combustion activities at evenings can also play a role. It is worth noting that the early-morning rush-hour peak on event days was smaller than on non-event days, which agrees with our earlier observation derived directly from experimental data (Salma et al., 2017) and is in line with the overall picture on urban NPF events (Zhang et al., 2015; Kulmala et al., 2017). On holidays, the modelled diurnal variation for non-event days contained an increasing part in the morning to a modest concentration level, which remains fairly constant over the daytime. This is explained by the differences in daily activities of citizens on workdays and holidays as far as both their intensity and timing are concerned.

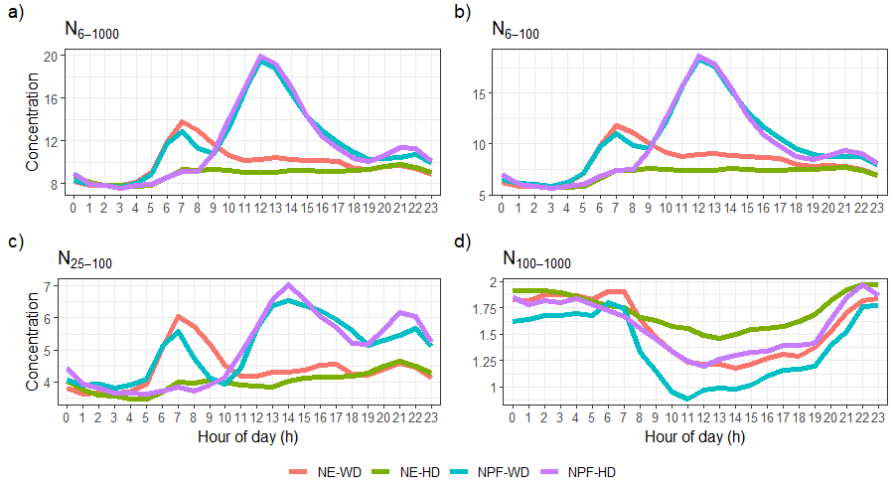


**Figure 3.** Diurnal patterns of particle number concentrations in the diameter ranges from 6 to 1000 nm ($N_{6–1000}$), from 6 to 100 nm ($N_{6–100}$), from 25 to 100 nm ($N_{25–100}$) and from 100 to 1000 nm ($N_{100–1000}$) in units of $10^3$ cm$^{-3}$. Red: non-event on workdays, green: non-event on holidays, cyan: event on workdays, purple: event on holidays.

The statistical diurnal patterns of $N_{6–1000}$ trends (Fig. 3a) were very similar or analogous to those of the $N_{6–100}$. These two size fractions are strongly connected with each other as explained in Sect. 3.1. The diurnal curves for $N_{25–100}$ (Fig. 3c) were also similar to the previous corresponding curves as far as the character and shape are concerned, while there were also evident differences between their relative

https://doi.org/10.5194/acp-2020-305
Preprint. Discussion started: 7 May 2020


Atmospheric Chemistry and Physics Discussions

structures. The peaks for the early morning and late afternoon rush hours were relatively larger than in the trends of 6–100- or 6–1000-nm size fractions due to the higher contribution of primary particles from high temperature sources in this size fraction. New particle formation generally occurs on days when $N_{25–100}$ are smaller before the event onset (between 08:00 and 11:00). The maximum of the peaks associated with NPF events in Fig. 3a and b – which is between 12:00 and 13:00 – was also shifted to later, i.e. to ca. 14:00 in Fig. 3c. This can be explained by the time needed for freshly nucleated particles to reach the diameter range >25 nm.

The statistical diurnal patterns for $N_{100–1000}$ seem very different from the smaller size ranges. First, their time variations were rather small in comparison to the other size fractions. On workdays, they only showed a modest elevation from 06:00 to 08:00 (morning rush hours), which is mainly caused by resuspension of road/surface dust particles by moving vehicles or by emissions of coarse particles from material wear. This morning peak was even missing on holidays, but another small and broad elevation showed up from 21:00 to 22:00. This and the overall changes during the daylight time are primarily related to the daily cycling of local meteorological conditions, in particular of boundary layer mixing height under stabile anti-cyclonic weather conditions, outlined above.

### 3.2.2 Effects of variables

Monthly mean coefficients (mean $v_m$ slopes in Eq. 4) of $NO_2$, $O_3$ and $SO_2$ derived by GLMM, which express their partial effects on particle number concentrations are shown in Fig. 4 for different size fractions.

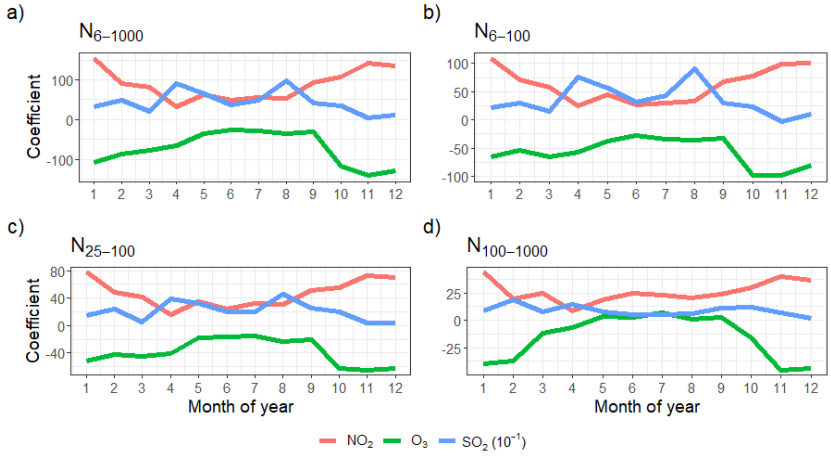


**Figure 4.** Distribution of monthly mean coefficients (which are proportional to the partial effects) for $NO_2$, $O_3$ and $SO_2$ on particle number concentrations separately in the diameter ranges from 6 to 1000 nm ($N_{6–1000}$), from 6 to 100 nm ($N_{6–100}$), from 25 to 100 nm ($N_{25–100}$) and from 100 to 1000 nm ($N_{100–1000}$).

https://doi.org/10.5194/acp-2020-305
Preprint. Discussion started: 7 May 2020


Atmospheric Chemistry and Physics Discussions

459 The coefficients of $SO_2$ and $NO_2$ are positive, while $O_3$ seems to have a decreasing effect on particle
460 number concentrations. The coefficients all have seasonal patterns, which means that the magnitude of
461 their effect on particle concentrations are of different magnitude in different months. This means for
462 example that 1 μg $m^{-3}$ increase in $NO_2$ concentration increases $N_{6–1000}$ concentration in January by 154
463 $m^{-3}$ but in June by 50 $m^{-3}$. This could, however, be partly caused by annual changes of boundary layer
464 mixing height or some other variable affecting particle concentrations, and correlating with these, but
465 not measured at the site. The boundary layer mixing height tends to be smaller in Budapest in winter
466 than in the other seasons (Salma et al., 2011), which ordinarily results in higher atmospheric
467 concentrations at steady-state absolute amounts of chemical species. The coefficients of $NO_2$ on $N_{6–1000}$,
468 $N_{6–100}$ and $N_{25–100}$ were higher in winter. This may indicate that large fractions of particles in these three
469 size fractions originate from residential heating and $NO_2$ acts as an indicator for this source. Another
470 major source of $NO_2$ and primary particles is the road traffic, but this does not show seasonal variation
471 in Budapest. The seasonal effect of $NO_2$ on chemically aged, regional type particles ($N_{100–1000}$) may not
472 be significant.

473 The partial effect of $O_3$ on $N_{6–1000}$, $N_{6–100}$ and $N_{25–100}$ was weaker in summer, late spring and early autumn.
474 This interval coincides with relatively large $O_3$ concentrations in the area. Ozone has a strong seasonal
475 variation (as shown in Fig. S1 in the Supplement). The negative correlation between $O_3$ concentration
476 and its effect on particle concentrations need further clarification since $O_3$ participates in a large variety
477 of complex atmospheric processes and also serves as a marker for photochemical processes which
478 influence secondary particle formation. The influence of $O_3$ on $N_{100–1000}$ was virtually negligible due
479 likely to the regional character of these particles (which are usually chemically aged and often represent
480 larger spatial scale due to their larger atmospheric residence time) similarly to $NO_2$. In addition, $O_3$
481 might act as an indicator of particulate pollution from traffic, power plants and other anthropogenic
482 sources. Then more ozone would indicate higher number of larger particles and due to coagulation less
483 smaller particles.

484 The partial effects of $SO_2$ on the particle number concentrations were the largest of the three gases
485 considered. In the $N_{6–1000}$, $N_{6–100}$ and $N_{25–100}$, two peaks appeared, one in spring and another one in late
486 summer. This shape is in line with the average distribution of the monthly mean relative NPF occurrence
487 frequency in Budapest (Salma and Németh, 2019). The latter distribution consists of an absolute and a
488 local minimum in January (with a monthly mean occurrence frequency of 5.9%) and in August (17.0%),
489 respectively, and an absolute and a local maximum in April (41%) and in September with (26%),
490 respectively. The distribution of the $SO_2$ coefficient suggests and confirms that $SO_2$, via NPF events
491 contribute in a substantial extent to the particle number concentrations in cities. The influence of $SO_2$
492 on $N_{100–1000}$ was virtually negligible due likely to the regional character of these particles similarly to the
493 other two gases included into the model.

https://doi.org/10.5194/acp-2020-305
Preprint. Discussion started: 7 May 2020


Atmospheric Chemistry and Physics Discussions

494 Figure 5 summarizes the effect of macro-circulation patterns on particle number concentrations in the
495 different size fractions. It is seen that the larger regional-type particles are less affected by the MCPs
496 than the smaller particles. The weather conditions favouring NPF events can be identified from the
497 curves by looking at the largest coefficients for size fraction of 6–100 nm.

https://doi.org/10.5194/acp-2020-305
Preprint. Discussion started: 7 May 2020


Atmospheric Chemistry and Physics Discussions

498 It seems that the MCP no. 3 (Mediterranean cyclone with a cold front over S Europe, N wind), 7 (highly
499 developed cyclone over N Europe, W wind) and 12 (anticyclone over the Carpathian Basin, changing
500 wind direction) can represent favourable conditions for NPF events than the other MCPs. Under these
501 conditions, the weather in the area is typically windy, with average solar radiation (expect for MCP no.
502 3 in summer when it shows low daily values), with strong planetary bounding layer evolution and
503 consequently, iv) the pollutants concentrations are below the average (expect for the winter inversions
504 in MCP no. 12). The air pollution situations are better separated by MCP codes in summer than in winter.
505 The weather type classified as no. 6 (Mediterranean cyclone with a warm front over S Europe, S wind)
506 disfavour the events. Under these conditions, the weather is typically cloudy and rainy with lower than
507 average solar radiation. This situation is often associated with polluted air in Budapest. Proportions for
508 NPF days for different MCP codes, which are shown Table S1 in the Supplement, also confirm these
509 conclusions.
510

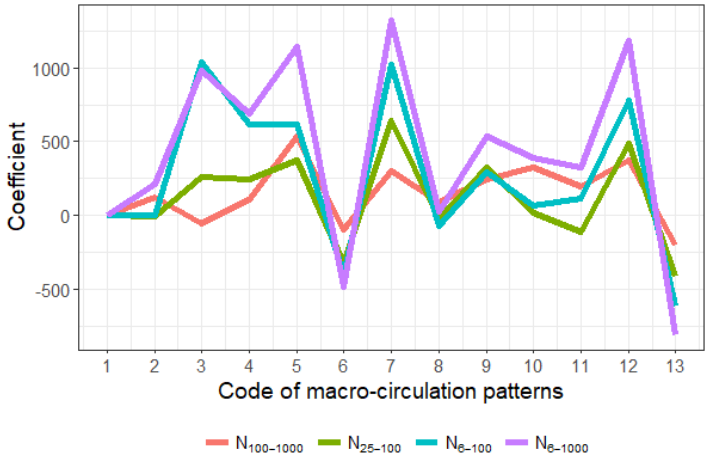


511
512 **Figure 5.** Distribution of monthly mean coefficients (which are proportional to the partial effects) for macro-
513 circulation patterns (Péczely codes) on particle number concentrations separately in the diameter ranges from 100
514 to 1000 nm ($N_{100–1000}$), from 25 to 100 nm ($N_{25–100}$), from 6 to 100 nm ($N_{6–100}$) and from 6 to 1000 nm ($N_{6–1000}$).

515 The coefficients for GRad and RH for different size fractions are shown in Fig. 6. It was found that these
516 variables do not have seasonal dependency, i.e. they contribute with equal strength to particle
517 concentrations throughout the year. Effect of GRad is positive for all size fractions, but it is weaker for
518 larger (regional-type or already chemically aged or processed) particles. The latter contribution could
519 be related to the bias in meteorological properties as well. The RH has negligible effect on size fraction
520 of 25–100 nm. It affects strongly and positively the largest particles, which means that the particles are
521 larger within higher humidity. This might be related to local meteorology, as higher RH probably means
522 more clouds and more clouds probably means less radiation and lower boundary layer and this could

https://doi.org/10.5194/acp-2020-305
Preprint. Discussion started: 7 May 2020


Atmospheric Chemistry and Physics Discussions

cause higher particle concentration. In contrast, the effect of RH on the smallest particles was negative, which is probably caused by high RHs, which limit NPF (e.g. Hamed et al., 2011).

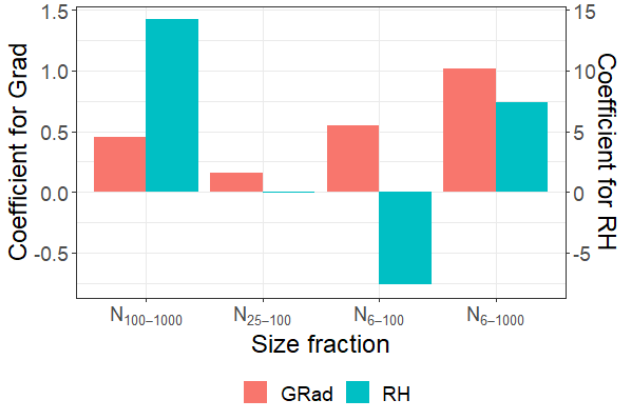


**Figure 6.** Distribution of monthly mean coefficients (which are proportional to the partial effects) for global radiation (GRad) and relative humidity (RH) separately in the diameter ranges from 100 to 1000 nm ($N_{100–1000}$), from 25 to 100 nm ($N_{25–100}$), from 6 to 100 nm ($N_{6–100}$) and from 6 to 1000 nm ($N_{6–1000}$).

### 3.2.3 Goodness-of-fit evaluation for GLMM

In order to estimate the uncertainty of the models for different size fractions, we calculated the mean absolute errors relative to the dependent variable mean, given by Willmot et al. (2009):

$$Err = (n^{-1} \sum_{i=1}^{n} |y_i - \hat{y}_i|) \cdot \bar{y}^{-1} , \quad (5)$$

where $n$ is the number of observations, $y_i$ are the observed particle number concentrations, $\hat{y}_i$ are the predicted values given by the GLMM and $\bar{y}$ is the mean of the observed values. In addition, we calculated Spearman's rank correlation coefficients between the observed and predicted values for all size fractions. Both goodness-of-fit estimates are shown in Table 4. As the relative errors for different size fractions are within a range of 0.30–0.34 and the correlations are higher than 0.70, it can be concluded that the model fitted the data with this size and measurement uncertainty well.

**Table 4.** Goodness-of-fit estimates for GLMM as expressed by the mean absolute error relative to the dependent variable mean and by Spearman's rank correlation coefficient separately in the size fractions of 6–1000, 6–100, 25–100 and 100–1000 nm.

| Size fraction | Error | Correlation |
|---|---|---|
| 6–1000 | 0.30 | 0.73 |
| 6–100 | 0.32 | 0.72 |
| 25–100 | 0.34 | 0.71 |
| 100–1000 | 0.34 | 0.73 |

https://doi.org/10.5194/acp-2020-305
Preprint. Discussion started: 7 May 2020


Atmospheric Chemistry and Physics Discussions

Figure 7 illustrates how well the GLMM model predicts the observations in all size fractions within a randomly selected period of one week in March 2015. The figure shows that the predicted values follow the observations fairly well in all size fractions. Overall, the statistical model finds the peaks of the concentration, but slightly underestimates the highest peaks and the fastest fluctuations and in some cases, overestimates the lowest concentrations.

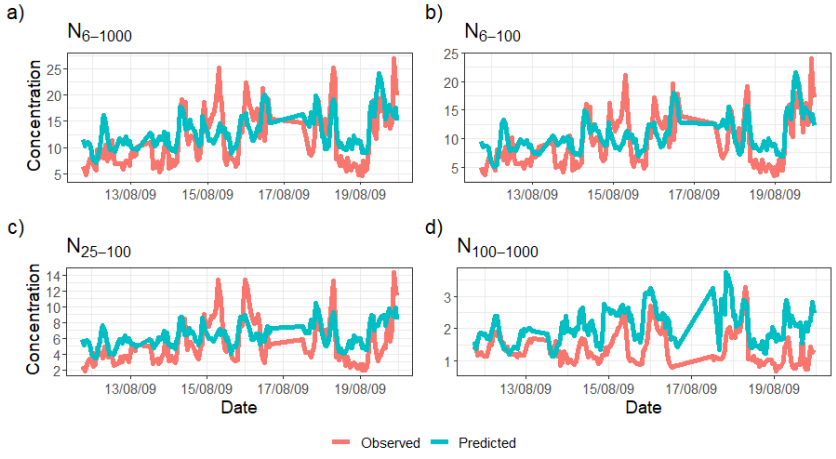


**Figure 7.** Observed (red line) and predicted (cyan line) time series for an illustrative example period separately in the size fractions of 6–1000, 6–100, 25–100 and 100–1000 nm.

## 4 Conclusions

In the present study, we determined decennial statistical time trends and diurnal statistical patterns of atmospheric particle number concentrations in various relevant size fractions in the city centre of Budapest in an interval of 2008–2018. The decennial statistical trends showed decreasing character except for the size fraction representing the regional. The mean overall decrease rate was approximately –5% scaled for the 10-year measurement interval. The decline can be interpreted as a consequence of the decreased anthropogenic emissions in the city. The diurnal statistical patterns suggested that reduced traffic emissions were most likely an important factor in causing the observed changes. It is expected that traffic intensity changed in a modest manner in the city centre during the time interval of interest, so our results indicate that the reductions is most likely related to lower emission factors. This appears to follow some changes of sulfur content in fuels and control measures on emissions for on-road heavy-duty diesel vehicles. Introduction of better particle filters in diesel cars, cleaner fuel and more sophisticated diesel engines could also contribute. The changes appear to have responded to both the policy on urban air quality and the influence of economic circumstances of inhabitants. Excitingly, the mean ages of passenger cars and busses in Hungary increased during the years under investigation. The exact explanation of the decrease requires continuation of the related measurements and further

https://doi.org/10.5194/acp-2020-305
Preprint. Discussion started: 7 May 2020


Atmospheric Chemistry and Physics Discussions

dedicated studies. The present results can be also used for evaluating the effectiveness of present and prospective mitigation policies.

The diurnal statistical patterns can be also utilized in interpreting some properties of NPF events in urban environments, and in explaining time evolution of particle number concentration. As a result of GLMM, we could, for instance, give a parametrization for predicting particle concentrations in different size fractions. Models similar to those developed in the present study could be used for other particle sizes or locations as well. The same parameterization cold be used at least in areas with similar concentration levels of particles and pollutants, while the extrapolation of the results to cleaner or more polluted environments needs to be confirmed before the use. Conjugate or linked parameterizations to be developed for varying environments can be implemented as a part of atmospheric models to predict the concentrations of climatically active particles in order to reduce their extensive computational times. In addition, this could also contribute to solving some current uncertain issues in the theoretical description of NPF and growth process, particularly when predicting cloud condensation nuclei concentrations.

**Data availability.** The observational data used in this paper are available on request from the corresponding author Imre Salma.

**Author contributions.** IS and SM formulated the original concept; ZN, VV, TW and IS collected and processed the experimental data; SM, VL and TY were responsible for the statistical data analyses and their physical basis; SM and IS interpreted the results; IS and SM wrote the manuscript with contributions from all co-authors.

**Competing interest.** The authors declare that they have no conflict of interest.

**Financial support.** The research was supported by the National Research, Development and Innovation Office, Hungary (contracts K116788, PD124283 and K132254), by the János Bolyai Research Scholarship of the Hungarian Academy of Sciences (ZN) and by the European Regional Development Fund and the Hungarian Government (GINOP-2.3.2-15-2016-00028), The Nessling Foundation, The Academy of Finland Centre of Excellence (grant no. 307331) and The Academy of Finland Competitive funding to strengthen university research profiles (PROFI) for the University of Eastern Finland (grant no. 325022) and Academy of Finland project (grant no. 299544)

## References

Aalto, P., Hämeri, K., Becker, E., Weber, R., Salm, J., Mäkelä, J., Hoell, C., O'Dowd, C., Karlsson, H., Väkevä, M., Koponen, I. K., Buzorius, G., and Kulmala, M.: Physical characterization of aerosol particles during nucleation events, Tellus, 53B, 344–358, 2001.

Aalto, P., Hämeri, K., Paatero, P., Kulmala, M., Bellander, T., Berglind, N., Bouso, L., Castaño-Vinyals, G., Sunyer, J., Cattani, G., Marconi, A., Cyrys, J., von Klot, S., Peters, A., Zetzsche, K., Lanki, T., Pekkanen, J., Nyberg, F., Sjövall, B., and Forastiere, F.: Aerosol particle number concentration measurements in five European cities using TSI-3022 condensation particle counter over a three-year period during health effects of air pollution on susceptible subpopulations, J. Air Waste Manage. Assoc., 55, 1064–1076, 2005.

https://doi.org/10.5194/acp-2020-305
Preprint. Discussion started: 7 May 2020


Atmospheric Chemistry and Physics Discussions

602 Asmi, A., Collaud Coen, M., Ogren, J. A., Andrews, E., Sheridan, P., Jefferson, A., Weingartner, E., Baltensperger,
603 U., Bukowiecki, N., Lihavainen, H., Kivekas, N., Asmi, E., Aalto, P. P., Kulmala, M., Wiedensohler, A.,
604 Birmili, W., Hamed, A., O'Dowd, C., Jennings, S. G., Weller, R., Flentje, H., Fjaeraa, A. M., Fiebig, M., Myhre,
605 C. L., Hallar, A. G., Swietlicki, E., Kristensson, A., and Laj, P.: Aerosol decadal trends - Part 2: In-situ aerosol
606 particle number concentrations at GAW and ACTRIS stations, Atmos. Chem. Phys., 13, 895–916, 2013.
607 Avino, P., Casciardi, S., Fanizza, C., and Manigrasso, M.: Deep investigation of ultrafine particles in urban air,
608 Aerosol Air Qual. Res., 11, 654–663, 2011.
609 Birmili, W., Wiedensohler, A., Heintzenberg, J., and Lehmann, K.: Atmospheric particle number size distribution
610 in central Europe: Statistical relations to air masses and meteorology, J. Geophys. Res., Atmospheres,
611 106(D23), 32005-18, 2001.
612 Braakhuis, H. M., Park, M. V., Gosens, I., De Jong, W. H., and Cassee, F. R.: Physicochemical characteristics of
613 nanomaterials that affect pulmonary inflammation, Part. Fibre Toxicol., 11:18, doi: 10.1186/1743-8977-11-18,
614 2014.
615 Brines, M., Dall'Osto, M., Beddows, D. C. S., Harrison, R. M., Gómez-Moreno, F., Núñez, L., Artíñano, B.,
616 Costabile, F., Gobbi, G. P., Salimi, F., Morawska, L., Sioutas, C., and Querol, X.: Traffic and nucleation events
617 as main sources of ultrafine particles in high-insolation developed world cities, Atmos. Chem. Phys. 15, 5929–
618 5945, 2015.
619 Cassee, F. R., Héroux, M.-E., Gerlofs-Nijland, M. E., and Kelly, F. J.: Particulate matter beyond mass: recent
620 health evidence on the role of fractions, chemical constituents and sources of emission, Inhal. Toxicol. 25,
621 802–812, 2013.
622 Carslaw, K. S., Lee, L. A., Reddington, C. L., Pringle, K. J., Rap, A., Forster, P. M., Mann, G. W., Spracklen, D.
623 V., Woodhouse, M. T., Regayre, L. A., and Pierce, J. R: Large contribution of natural aerosols to uncertainty
624 in indirect forcing, Nature, 503, 67–71, 2013.
625 Dada, L., Ylivinkka, I., Baalbaki, R., Li, Ch., Guo, Y., Yan, Ch., Yao, L., Sarnela, N., Jokinen, T., Daellenbach,
626 K. D., Yin, R., Deng, Ch., Chu, B., Nieminen, T., Kontkanen, J., Stolzenburg, D., Sipilä, M., Hussein, T.,
627 Paasonen, P., Bianchi, F., Salma, I., Weidinger, T., Pikridas, M., Sciare, J., Jiang, J., Liu, Y., Petäjä, T.,
628 Kerminen, V.-M., and Kulmala, M.: Sources and sinks driving sulphuric acid concentrations in contrasting
629 environments: implications on proxy calculations, Atmos. Chem. Phys. Discuss., under evaluation, 2020.
630 Dal Maso, M., Kulmala, M., Lehtinen, K. E. J., Mäkelä, J. M., Aalto, P. P., and O'Dowd, C.: Condensation and
631 coagulation sinks and formation of nucleation mode particles in coastal and boreal forest boundary layers, J.
632 Geophys. Res., 107(19D), 8097, 10.1029/2001jd001053, 2002.
633 Dal Maso, M., Kulmala, M., Riipinen, I., Wagner, R., Hussein, T., Aalto, P. P., and Lehtinen, K. E. J.: Formation
634 and growth of fresh atmospheric aerosols: eight years of aerosol size distribution data from SMEAR II,
635 Hyytiälä, Finland, Boreal Environ. Res., 10, 323–336, 2005.
636 Dall'Osto, M., Querol, X., Alastuey, A., O'Dowd, C., Harrison, R. M., Wenger, J., and Gómez-Moreno, F. J.: On
637 the spatial distribution and evolution of ultrafine particles in Barcelona, Atmos. Chem. Phys., 13, 741–759,
638 2013.
639 Directive 2009/30/EC, Official Journal of the European Union, L 140, EN, 88–113, 5. 6. 2009.
640 Dunne, E. M., Gordon, H., Kürten, A., Almeida, J., Duplissy, J., Williamson, C., Ortega, I. K., Pringle, K. J.,
641 Adamov, A., Baltensperger, U., Barmet, P., Benduhn, F., Bianchi, F., Breitenlechner, M., Clarke, A., Curtius,
642 J., Dommen, J., Donahue, N. M., Ehrhart, S., Flagan, R. C., Franchin, A., Guida, R., Hakala, J., Hansel, A.,
643 Heinritzi, M., Jokinen, T., Kangasluoma, J., Kirkby, J., Kulmala, M., Kupc, A., Lawler, M. J., Lehtipalo, K.,
644 Makhmutov, V., Mann, G., Mathot, S., Merikanto, J., Miettinen, P., Nenes, A., Onnela, A., Rap, A.,
645 Reddington, C. L. S., Riccobono, F., Richards, N. A. D., Rissanen, M. P., Rondo, L., Sarnela, N.,
646 Schobesberger, S., Sengupta, K., Simon, M., Sipilä, M., Smith, J. N., Stozkhov, Y., Tomé, A., Tröstl, J.,
647 Wagner, P. E., Wimmer, D., Winkler, P. M., Worsnop, D. R., and Carslaw, K. S.: Global atmospheric particle
648 formation from CERN CLOUD measurements, Science 354, 1119–1124, 2016.
649 Durbin, J. and Koopman, S. J.: Time series analysis by state space methods, Oxford University Press, Oxford,
650 2012.
651 Giechaskiel, B., Lahde, T., Suarez-Bertoa, R., Clairotte, M., Grigoratos, T., Zardini, A., Perujo, A., and Martini,
652 G.: Particle number measurements in the European legislation and future JRC activities, Combustion Engines,
653 174, 3–16, 2018.

https://doi.org/10.5194/acp-2020-305
Preprint. Discussion started: 7 May 2020


Atmospheric Chemistry and Physics Discussions

654 Gordon, H., Sengupta, K., Rap, A., Duplissy, J., Frege, C., Williamson, C., Heinritzi, M., Simon, M., Yan, C.,
655 Almeida, J., Tröstl, J., Nieminen, T., Ortega, I. K., Wagner, R., Dunne, E. M., Adamov, A., Amorim, A.,
656 Bernhammer, A. K., Bianchi, F., Breitenlechner, M., Brilke, S., Chen, X., Craven, J. S., Dias, A., Ehrhart, S.,
657 Fischer, L., Flagan, R. C., Franchin, A., Fuchs, C., Guida, R., Hakala, J., Hoyle, C. R., Jokinen, T., Junninen,
658 H., Kangasluoma, J., Kim, J., Kirkby, J., Krapf, M., Kürten, A., Laaksonen, A., Lehtipalo, K., Makhmutov, V.,
659 Mathot, S., Molteni, U., Monks, S. A., Onnela, A., Peräkylä, O., Piel, F., Petäjä, T., Praplan, A. P., Pringle, K.
660 J., Richards, N. A. D., Rissanen, M. P., Rondo, L., Sarnela, N., Schobesberger, S., Scott, C. E., Seinfeld, J. H.,
661 Sharma, S., Sipilä, M., Steiner, G., Stozhkov, Y., Stratmann, F., Tomé, A., Virtanen, A., Vogel, A. L., Wagner,
662 A. C., Wagner, P. E., Weingartner, E., Wimmer, D., Winkler, P. M., Ye, P., Zhang, X., Hansel, A., Dommen,
663 J., Donahue, N. M., Worsnop, D. R., Baltensperger, U., Kulmala, M., Curtius, J., and Carslaw, K. S.: Reduced
664 anthropogenic aerosol radiative forcing caused by biogenic new particle formation, Proc. Natl. Acad. Sci.
665 U.S.A., 113, 12053–12058, 2016.
666 Guo, H., Wang, D. W., Cheung, K., Ling, Z. H., Chan, C. K., and Yao, X. H.: Observation of aerosol size
667 distribution and new particle formation at a mountain site in subtropical Hong Kong, Atmos. Chem. Phys., 12,
668 9923–9939, https://doi.org/10.5194/acp-12-9923-2012, 2012.
669 Hamed, A., H. Korhonen, S.-L. Sihto, J. Joutsensaari, H. Järvinen, T. Petäjä, F. Arnold, T. Nieminen, M. Kulmala,
670 J. N. Smith, K. E. J. Lehtinen, A. Laaksonen: The role of relative humidity in continental new particle
671 formation, J. Geophys. Res., 116, D03202, doi:10.1029/2010JD014186, 2011.
672 Hussein, T., Puustinen, A., Aalto, P. P., Mäkelä, J. M., Hämeri, K., and Kulmala, M.: Urban aerosol number size
673 distributions, Atmos. Chem. Phys., 4, 391–411, 2004.
674 Hyvönen, S., Junninen, H., Laakso, L., Dal Maso, M., Grönholm, T., Bonn, B., Keronen, P., Aalto, P., Hiltunen,
675 V., Pohja, T., Launiainen, S., Hari, P., Mannila, H., and Kulmala, M.: A look at aerosol formation using data
676 mining techniques, Atmos. Chem. Phys., 5, 3345–3356, 2005.
677 Károssy, Cs.: A Kárpát-medence Péczely-féle makroszinoptikus időjárási helyzeteinek katalógusa 1881–2015
678 (Catalogue of the Péczely macrosynoptic weather types for the Carpathian Basin 1881–2015, in Hungarian),
679 OSKAR Kiadó, Budapest, 2016.
680 Kerminen, V.-M., Paramonov, M., Anttila, T., Riipinen, I., Fountoukis, C., Korhonen, H., Asmi, E., Laakso, L.,
681 Lihavainen, H., Swietlicki, E., Svenningsson, B., Asmi, A., Pandis, S. N., Kulmala, M., and Petäjä, T.: Cloud
682 condensation nuclei production associated with atmospheric nucleation: a synthesis based on existing literature
683 and new results, Atmos. Chem. Phys., 12, 12037–12059, 2012.
684 Kerminen, V.-M., Chen, X., Vakkari, V., Petäjä, T., Kulmala, M., and Bianchi, F.: Atmospheric new particle
685 formation and growth: review of field observations, Environ. Res. Lett., 13 (2018) 103003, 2018.
686 KSH, National register of road vehicles (in Hungarian), Hungarian Central Statistical Office, Budapest, 2019.
687 Kulmala, M., Dal Maso, M., Mäkelä, J. M., Pirjola, L., Väkevä, M., Aalto, P., Miikkulainen, P., Hämeri, K., and
688 O'Dowd, C. D.: On the formation, growth and composition of nucleation mode particles, Tellus B53, 479–490,
689 2001.
690 Kulmala, M., Petäjä, T., Nieminen, T., Sipilä, M., Manninen, H. E., Lehtipalo, K., Dal Maso, M., Aalto, P. P.,
691 Junninen, H., Paasonen, P., Riipinen, I., Lehtinen, K. E. J., Laaksonen, A., and Kerminen, V.-M.: Measurement
692 of the nucleation of atmospheric aerosol particles, Nat. Protoc., 7, 1651–1667, doi:10.1038/nprot.2012.091,
693 2012.
694 Kulmala, M., Kontkanen, J., Junninen, H., Lehtipalo, K., Manninen, H. E., Nieminen, T., Petäjä, T., Sipilä, M.,
695 Schobesberger, S., Rantala, P., Franchin, A., Jokinen, T., Järvinen, E., Äijälä, M., Kangasluoma, J., Hakala, J.,
696 Aalto, P. P., Paasonen, P., Mikkilä, J., Vanhanen, J., Aalto, J., Hakola, H., Makkonen, U., Ruuskanen, T.,
697 Mauldin, R. L. III, Duplissy, J., Vehkamäki, H., Bäck, J., Kortelainen, A., Riipinen, I., Kurtén, T., Johnston,
698 M. V., Smith, J. N., Ehn, M., Mentel, T. F., Lehtinen, K. E. J., Laaksonen, A., Kerminen, V.-M., and Worsnop,
699 D. R.: Direct observations of atmospheric aerosol nucleation, Science, 339, 943–946, 2013.
700 Kulmala, M., Petäjä, T., Ehn, M., Thornton, J., Sipilä, M., Worsnop, D. R., and Kerminen, V.-M.: Chemistry of
701 atmospheric nucleation: On the recent advances on precursor characterization and atmospheric cluster
702 composition in connection with atmospheric new particle formation, Annu. Rev. Phys. Chem., 65, 21−37,
703 2014.
704 Kulmala, M., Kerminen, V. M., Petäjä, T., Ding, A. J., and Wang, L.: Atmospheric gas-to-particle conversion:
705 why NPF events are observed in megacities, Faraday Discuss., doi:10.1039/C6FD00257A, 2017.



706 Laine, M.: Introduction to Dynamic Linear Models for Time Series Analysis. In: Montillet, J. P., Bos, M. (eds),
707 Geodetic Time Series Analysis in Earth Sciences, Springer, pp. 139–156, 2020.
708 Maheras, P., Tolika, K., Tegoulias, I., Anagnostopoulou, Ch., Szpirosz, K. Károssy, Cs., and Makra, L.:
709 Comparison of an automated classification system with an empirical classification of circulation patterns over
710 the Pannonian basin, Central Europe, Meteorol. Atmos. Phys., https://doi.org/10.1007/s00703-018-0601-x,
711 2018.
712 Makkonen, R., Asmi, A., Korhonen, H., Kokkola, H., Järvenoja, S., Räisänen, P., Lehtinen, K. E. J., Laaksonen,
713 A., Kerminen, V.-M., Järvinen, H., Lohmann, U., Bennartz, R., Feichter, J., and Kulmala, M.: Sensitivity of
714 aerosol concentrations and cloud properties to nucleation and secondary organic distribution in ECHAM5-
715 HAM global circulation model, Atmos. Chem. Phys., 9, 1747–1766, 2009.
716 Masiol, M., Squizzato, S., Chalupa, D., Utell, M. J., Rich, D. Q., and Hopke, P. K.: Long-term trends in submicron
717 particle concentrations in a metropolitan area of the northeastern United States, Sci. Total Environ., 633, 59–
718 70, 2018.
719 McCulloch, C. E., Searle, S. R., and Neuhaus, J. M.: Generalized, linear, and mixed models, 2nd ed., Wiley, New
720 York, 2008.
721 McFiggans, G., Mentel, T. F., Wildt, J., Pullinen, I., Kang, S., Kleist, E., Schmitt, S., Springer, M., Tillmann, R.,
722 Wu, C., Zhao, D., Hallquist, M., Faxon, C., Le Breton, M., Hallquist, A. M., Simpson, D., Bergstroem, R.,
723 Jenkin, M. E., Ehn, M., Thornton, J. A., Alfarra, M. R., Bannan, T. J., Percival, C. J., Priestley, M., Topping,
724 D., and Kiendler-Scharr, A.: Secondary organic aerosol reduced by mixture of atmospheric vapours, Nature,
725 565, 587–593, 2019.
726 Merikanto, J., Spracklen, D. V., Mann, G. W., Pickering, S. J., and Carslaw, K. S.: Impact of nucleation on global
727 CCN, Atmos. Chem. Phys., 9, 8601–8616, 2009.
728 Mikkonen, S., Lehtinen, K. E. J., Hamed, A., Joutsensaari, J., Facchini, M. C., and Laaksonen, A.: Using
729 discriminant analysis as a nucleation event classification method, Atmos. Chem. Phys., 6, 5549–5557,
730 https://doi.org/10.5194/acp-6-5549-2006, 2006.
731 Mikkonen, S., Korhonen, H., Romakkaniemi, S., Smith, J. N., Joutsensaari, J., Lehtinen, K. E. J., Hamed, A.,
732 Breider, T. J., Birmili, W., Spindler, G., Plass-Duelmer, C., Facchini, M. C., and Laaksonen, A.:
733 Meteorological and trace gas factors affecting the number concentration of atmospheric Aitken ($D_p$=50 nm)
734 particles in the continental boundary layer: parameterization using a multivariate mixed effects model, Geosci.
735 Model Dev., 4, 1–13, https://doi.org/10.5194/gmd-4-1-2011, 2011a.
736 Mikkonen, S., Romakkaniemi, S., Smith, J. N., Korhonen, H., Petäjä, T., Plass-Duelmer, C., Boy, M., McMurry,
737 P. H., Lehtinen, K. E. J., Joutsensaari, J., Hamed, A., Mauldin III, R. L., Birmili, W., Spindler, G., Arnold, F.,
738 Kulmala, M., and Laaksonen, A.: A statistical proxy for sulphuric acid concentration, Atmos. Chem. Phys., 11
739 11319–11334, https://doi.org/10.5194/acp-11-11319-2011, 2011b.
740 Mikkonen, S., Laine, M., Mäkelä, H. M., Gregow, H., Tuomenvirta, H., Lahtinen, M., Laaksonen, A.: Trends in
741 the average temperature in Finland, 1847-2013, Stoch. Environ. Res. Risk Ass., 29, 1521–1529, 2015.
742 Moore, K. F., Ning, Z., Ntziachristos, L., Schauer, J. J., and Sioutas, C.: Daily variation in the properties of urban
743 ultrafine aerosol - Part I: Physical characterization and volatility, Atmos. Environ., 41, 8633–8646, 2007.
744 Moosmuller, H., Chakrabarty, R. K. and Arnott, W: Aerosol light absorption and its measurement: A review, J.
745 Quant. Spectrosc. Radiat. Transf., 110, 844–878, 2009.
746 Németh, Z. and Salma, I.: Spatial extension of nucleating air masses in the Carpathian Basin, Atmos. Chem. Phys.,
747 14, 8841–8848, 2014.
748 Németh, Z., Rosati, B., Zíková, N., Salma, I., Bozó, L., Dameto de España, C., Schwarz, J., Ždímal, V., and
749 Wonaschütz, A.: Comparison of atmospheric new particle formation and growth events in three Central
750 European cities, Atmos. Environ., 178, 191–197, 2018.
751 Nieminen, T., Asmi, A., Dal Maso, M., P. Aalto, P., Keronen, P., Petäjä, T., Kulmala, M. & Kerminen, V.-M.:
752 Trends in atmospheric new-particle formation: 16 years of observations in a boreal-forest environment. Boreal
753 Env. Res. 19 (suppl. B): 191–214, 2014.
754 Nieminen, T., Kerminen, V.-M., Petäjä, T., Aalto, P. P., Arshinov, M., Asmi, E., Baltensperger, U., Beddows, D.
755 C. S., Beukes, J. P., Collins, D., Ding, A., Harrison, R. M., Henzing, B., Hooda, R., Hu, M., Hõrrak, U.,
756 Kivekäs, N., Komsaare, K., Krejci, R., Kristensson, A., Laakso, L., Laaksonen, A., Leaitch, W. R., Lihavainen,
757 H., Mihalopoulos, N., Németh, Z., Nie, W., O'Dowd, C., Salma, I., Sellegri, K., Svenningsson, B., Swietlicki,
758 E., Tunved, P., Ulevicius, V., Vakkari, V., Vana, M., Wiedensohler, A., Wu, Z., Virtanen, A., and Kulmala,

https://doi.org/10.5194/acp-2020-305
Preprint. Discussion started: 7 May 2020


Atmospheric Chemistry and Physics Discussions

M.: Global analysis of continental boundary layer new particle formation based on long-term measurements, Atmos. Chem. Phys., 18, 14737–14756, 2018.

Oberdörster, G., Oberdörster, E., and Oberdörster, J.: Nanotoxicology: an emerging discipline evolving from studies of ultrafine particles, Environ. Health Perspect., 113, 823–839, 2005.

Ohlwein, S., Kappeler, R., Joss, M. K., Künzli, N., and Hoffmann, B.: Health effects of ultrafine particles: a systematic literature review update of epidemiological evidence, Int. J. Public Health, 685, 547–559, 2019.

Ostro, B., Hu, J., Goldberg, D., Reynolds, P., Hertz, A., Bernstein, L., and Kleeman, M. J.: Associations of mortality with long-term exposures to fine and ultrafine particles, species and sources: results from the California teachers study cohort, Environ. Health Perspect., 123, 549–556, 2015.

Paasonen, P., Kupiainen, K., Klimont, Z., Visschedijk, A., Denier van der Gon, H. A. C., and Amann, M.: Continental anthropogenic primary particle number emissions, Atmos. Chem. Phys., 16, 6823–6840, 2016.

Péczely, Gy.: Grosswetterlagen in Ungarn (Large-scale weather situations in Hungary, in German), Publication of the Hungarian Meteorological Institute, 30, pp. 86, Budapest, 1957.

Petäjä, T., Mauldin, III, R. L., Kosciuch, E., McGrath, J., Nieminen, T., Paasonen, P., Boy, M., Adamov, A., Kotiaho, T., and Kulmala, M.: Sulfuric acid and OH concentrations in a boreal forest site, Atmos. Chem. Phys., 9, 7435–7448, 2009.

Petris, G., Petrone, S., and Campagnoli, P.: Dynamic linear models, Springer, New York, 2009.

Pinheiro, J.C., and Bates, D.M.: Mixed-Effects Models in S and S-PLUS, Springer, 2000.

Pöschl, U., Rudich, Y., and Ammann, M.: Kinetic model framework for aerosol and cloud surface chemistry and gas-particle interactions – Part 1: General equations, parameters, and terminology, Atmos. Chem. Phys., 7, 5989–6023, 2007.

Raes, F., Van Dingenen, R., Vignati, E., Wilson, J., Putaud, J. P., Seinfeld, J. H., and Adams, P.: Formation and cycling of aerosol in the global troposphere, Atmos. Environ., 34, 4215–4240, 2000.

Rich, D. Q., Zareba, W., Beckett, W., Hopke, P. K., Oakes, D., Frampton, M. W., Bisognano, J., Chalupa, D., Bausch, J., O'Shea, K., Wang, Y., and Utell, M. J.: Are ambient ultrafine, accumulation mode, and fine particles associatedwith adverse cardiac responses in patients undergoing cardiac rehabilitation?, Environ. Health Perspect., 120, 1162–1169, 2012.

Saha, P. K., Robinson, E. S., Shah, R. U., Zimmerman, N., Apte, J. S., Robinson, A. L., and Presto, A. A.: Reduced ultrafine particle concentration in urban air: changes in nucleation and anthropogenic emissions, Environ. Sci. Technol., 52, 6798−6806, 2018.

Salma, I., Borsós, T., Weidinger, T., Aalto, P., Hussein, T., Dal Maso, M., and Kulmala, M.: Production, growth and properties of ultrafine atmospheric aerosol particles in an urban environment, Atmos. Chem. Phys., 11, 1339–1353, 2011.

Salma, I., Borsós, T., Németh, Z., Weidinger, T., Aalto, T., and Kulmala, M.: Comparative study of ultrafine atmospheric aerosol within a city, Atmos. Environ., 92, 154–161, 2014.

Salma, I., Németh, Z., Weidinger, T., Kovács, B., and Kristóf, G.: Measurement, growth types and shrinkage of newly formed aerosol particles at an urban research platform, Atmos. Chem. Phys., 16, 7837–7851, 2016a.

Salma, I., Németh, Z., Kerminen, V. M., Aalto, P., Nieminen, T., Weidinger, T., Molnár, Á., Imre, K., and Kulmala, M.: Regional effect on urban atmospheric nucleation, Atmos. Chem. Phys., 16, 8715–8728, 2016b.

Salma, I., Varga, V., and Németh, Z.: Quantification of an atmospheric nucleation and growth process as a single source of aerosol particles in a city, Atmos. Chem. Phys., 17, 15007–15017, 2017.

Salma, I. and Németh, Z.: Dynamic and timing properties of new aerosol particle formation and consecutive growth events, Atmos. Chem. Phys., 19, 5835–5852, 2019.

Salvo, A., Brito, J., Artaxo, P., and Geiger, F. M.: Reduced ultrafine particle levels in São Paulo's atmosphere during shifts from gasoline to ethanol use, Nat. Commun., 8, 77, DOI: 10.1038/s41467-017-00041-5, 2017.

Schmid, O. and Stoeger, T.: Surface area is the biologically most effective dose metric for acute nanoparticle toxicity in the lung, J. Aerosol Sci., 99, 133–143, 2016.

Sihto, S.-L., Mikkilä, J., Vanhanen, J., Ehn, M., Liao, L., Lehtipalo, K., Aalto, P. P., Duplissy, J., Petäjä, T., Kerminen, V.-M., Boy, M., and Kulmala, M.: Seasonal variation of CCN concentrations and aerosol activation properties in boreal forest, Atmos. Chem. Phys., 11, 13269–13285, 2011.

Sipilä, M., Berndt, T., Petäjä, T., Brus, D., Vanhanen, J., Stratmann, F., Patokoski, J., Mauldin, R. L. 3rd, Hyvärinen, A. P., Lihavainen, H., and Kulmala, M.: The role of sulfuric acid in atmospheric nucleation, Science, 327(5970), 1243-6. doi: 10.1126/science.1180315, 2010.

https://doi.org/10.5194/acp-2020-305
Preprint. Discussion started: 7 May 2020


Atmospheric Chemistry and Physics Discussions

812 Spracklen, D. V., Carslaw, K. S., Merikanto, J., Mann, G. W., Reddington, C. L., Pickering, S., Ogren, J. A.,
813 Andrews, E., Baltensperger, U., Weingartner, E., Boy, M., Kulmala, M., Laakso, L., Lihavainen, H., Kivekäs,
814 N., Komppula, M., Mihalopoulos, N., Kouvarakis, G., Jennings, S. G., O'Dowd, C., Birmili, W., Wiedensohler,
815 A., Weller, R., Gras, J., Laj, P., Sellegri, K., Bonn, B., Krejčí, R., Laaksonen, A., Hamed, A., Minikin, A.,
816 Harrison, R. M., Talbot, R., and Sun, J.: The contribution of boundary layer nucleation events to total particle
817 concentrations on regional and global scales, Atmos. Chem. Phys., 6, 5631–5648, 2006.
818 Sun, J., Birmili, W., Hermann, M., Tuch, T., Weinhold, K., Merkel, M., Rasch, F., Müller, T., Schladitz, A.,
819 Bastian, S., Löschau, G., Cyrys, J., Gu, J., Flentje, H., Briel, B., Asbach, C., Kaminski, H., Ries, L., Sohmer,
820 R., Gerwig, H., Wirtz, K., Meinhardt, F., Schwerin, A., Bath, O., Ma, N., and Wiedensohler, A.: Decreasing
821 trends of particle number and black carbon mass concentrations at 16 observational sites in Germany from
822 2009 to 2018, Atmos. Chem. Phys. Discuss., doi:10.5194/acp-2019-754, 2019.
823 Wehner, B. and Wiedensohler, A.: Long term measurements of submicrometer urban aerosols: statistical analysis
824 for correlations with meteorological conditions and trace gases, Atmos. Chem. Phys., 3, 867–879, 2003
825 Wiedensohler, A., Cheng, Y. F., Nowak, A., Wehner, B., Achtert, P., Berghof, M., Birmili, W., Wu, Z. J., Hu, M.,
826 Zhu, T., Takegawa, N., Kita, K., Kondo, Y., Lou, S. R., Hofzumahaus, A., Holland, F., Wahner, A., Gunthe,
827 S. S., Rose, D., Su, H., and Pöschl, U.: Mobility particle size spectrometers: harmonization of technical
828 standards and data structure to facilitate high quality long-term observations of atmospheric particle number
829 size distributions, Atmos. Meas. Tech., 5, 657–685, 2012.
830 Willmott, C. J., Matsuura, K., and Robeson, S. M.: Ambiguities inherent in sums-of-squares-based error statistics,
831 Atmos. Environ., 43, 749–752, doi:10.1016/j.atmosenv.2008.10.005, 2009.
832 Yu, F., Luo, G., Bates, T. S., Anderson, B., Clarke, A., Kapustin, V., Yantosca, R. M., Wang, Y., and Wu, S.:
833 Spatial distributions of particle number concentrations in the global troposphere: simulations, observations,
834 and implications for nucleation mechanisms, J. Geophys. Res., 115, D17205, doi:10.1029/2009JD013473,
835 2010.
836 Zaidan, M. A., Haapasilta, V., Relan, R., Paasonen, P., Kerminen, V.-M., Junninen, H., Kulmala, M., and Foster,
837 A. S.: Exploring non-linear associations between atmospheric new-particle formation and ambient variables: a
838 mutual information approach, Atmos. Chem. Phys., 18, 12699–12714, 2018.
839 Zhang, R., Wang, G., Guo, S., Zamora, M. L., Ying, Q., Lin, Y., Wang, W., Hu, M., and Wang, Y.: Formation of
840 urban fine particulate matter, Chem. Rev., 115, 3803−3855, 2015.